On the Speed of the Eddy-Driven Jet and the Width of the Hadley Cell in the Southern Hemisphere

PAULO CEPPI AND DENNIS L. HARTMANN

Department of Atmospheric Sciences, University of Washington, Seattle, Washington

(Manuscript received 11 July 2012, in final form 12 October 2012)

ABSTRACT

A strong correlation between the speed of the eddy-driven jet and the width of the Hadley cell is found to exist in the Southern Hemisphere, both in reanalysis data and in twenty-first-century integrations from the Intergovernmental Panel on Climate Change (IPCC) Fifth Assessment Report multimodel archive. Analysis of the space–time spectra of eddy momentum flux reveals that variations in eddy-driven jet speed are related to changes in the mean phase speed of midlatitude eddies. An increase in eddy phase speeds induces a poleward shift of the critical latitudes and a poleward expansion of the region of subtropical wave breaking. The associated changes in eddy momentum flux convergence are balanced by anomalous meridional winds consistent with a wider Hadley cell. At the same time, faster eddies are also associated with a strengthened poleward eddy momentum flux, sustaining a stronger westerly jet in midlatitudes. The proposed mechanism is consistent with the seasonal dependence of the interannual variability of the Hadley cell width and appears to explain at least part of the projected twenty-first-century trends.

1. Introduction

One of the most salient features of Earth's general circulation is the presence of Hadley cells (HCs) in the tropical belts of both hemispheres. Associated with their large-scale motions are some of the main characteristics of tropical and subtropical climates: the intertropical convergence zone in the rising branch and the subtropical dry zones in the descending branches (e.g., Hartmann 1994). Studying the factors determining the meridional extent of these overturning circulations is therefore essential to understand the spatial distribution of tropical and subtropical climates and its changes.

The role of the HCs is particularly crucial in the context of climate change and the observed widening of the atmospheric circulation. Observations show a poleward shift of the eddy-driven jets and an expansion of the HCs in recent decades, particularly in the Southern Hemisphere (Hu and Fu 2007; Johanson and Fu 2009; Lu et al. 2009), and the role of radiative forcings induced by greenhouse gases and stratospheric ozone has been shown to be crucial in this context (Polvani et al. 2011b; McLandress et al. 2011). Further, comprehensive general circulation model (GCM) simulations predict that this expansion will continue throughout the twenty-first century, assuming further increases in greenhouse gas concentrations. Such changes, if they occur, are likely to have dramatic impacts on the distribution of precipitation and on the moisture budget in the subtropics (Seidel et al. 2008).

In this paper, we address the question of how extratropical eddies may control the interannual variability of the HC width. It is worth summarizing some recent contributions to this question. Using idealized dry GCM experiments, Walker and Schneider (2006) demonstrated the importance of eddies in controlling the width and strength of the HCs in Earthlike climates. In a study comparing the effects of El Niño–Southern Oscillation (ENSO) versus global warming, Lu et al. (2008) discussed the possible role of increasing eddy phase speeds in the predicted poleward expansion of the circulation as the climate warms. Recently, Kang and Polvani (2011) showed a strong relationship between the latitude of the eddy-driven jet and the edge of the HCs in Southern Hemispheric summer. Despite the existing body of work, however, we are not aware of any study that has provided a detailed mechanism explaining the interactions between eddies and the extent of the HCs on interannual time scales.

Corresponding author address: Paulo Ceppi, Department of Atmospheric Sciences, University of Washington, Box 351640, Seattle, WA 98195.
E-mail: ceppi@atmos.washington.edu

DOI: 10.1175/JCLI-D-12-00414.1

© 2013 American Meteorological Society

Here, we propose that interannual variations in the extent of the HCs can be modulated by variations in the phase speeds of extratropical waves. As discussed by Chen and Held (2007) and Chen et al. (2008), variations in eddy phase speeds may be the cause for shifts of the eddy-driven jet through changes in the critical latitudes of the waves. Our results support the view that the same mechanism may explain variations in HC extent on interannual time scales and possibly also long-term trends. In addition, such a mechanism provides a simple explanation for the observed seasonal differences in variability of the extent of the HCs.

2. Data and methods

a. Reanalysis data

We use monthly zonal and meridional wind data from the National Centers for Environmental Prediction (NCEP) reanalysis (Kalnay et al. 1996), covering the time period June 1948 to March 2012 (64 years) for the Southern Hemisphere (SH). Daily 1200 UTC data on the 250-hPa level are used to calculate eddy momentum fluxes and their power spectra as a function of latitude and phase speed. HC width and eddy-driven jet speeds are derived from monthly data, seasonally averaged over winter [June–September (JJAS)] and summer [December–March (DJFM)] months. To compare trends in HC width across reanalysis datasets, we also utilize 1979–2005 monthly European Centre for Medium-Range Weather Forecasts (ECMWF) Interim Re-Analysis (ERA-Interim) data (Dee et al. 2011), averaged in the same manner.

b. Model simulations

We analyze historical (1901–2005) simulations of 29 coupled GCMs from the archive of the Coupled Model Intercomparison Project, phase 5 (CMIP5; Taylor et al. 2012). Seasonally averaged zonal and meridional wind data are used to calculate the HC width and the eddy-driven jet speed as described below. In addition, twenty-first-century trends in the same quantities are estimated from 19 integrations based on the Representative Concentration Pathway 8.5 (RCP8.5) emission scenario. The models used are listed in Table 1.

To study the relationship between HC width and extratropical eddies in the absence of trends, we analyze zonal and meridional wind data from the preindustrial control experiment of the GFDL-ESM2G model, which is 500 years long. Daily instantaneous wind data at 1200 UTC are also used to calculate the latitude–phase speed power spectra of eddy momentum flux on the 250-hPa level.

c. Hadley cell width, eddy-driven jet speed, and latitude

The extent of the HC is calculated as the latitude where the mass streamfunction first reaches zero at 500 hPa poleward of the ascending branch of the HC. The mass streamfunction Ψ is determined by vertically integrating the pressure-weighted, zonally averaged meridional wind v:

$$\Psi = -\frac{2\pi a}{g}\int_0^p \overline{v}\cos\phi\, dp',$$

where φ represents latitude, a is the radius of Earth, and other symbols have the conventional meaning. A clockwise circulation (such as the Northern Hemispheric HC) is defined as negative, while counterclockwise circulations are positive. In this study, we compare the extent of the HC with the speed of the eddy-driven jet (hereafter $\phi_{\Psi 500}$ and $\mathrm{U850_{max}}$, respectively). $\mathrm{U850_{max}}$ is defined as the maximum westerly wind speed at 850 hPa. We also define the eddy-driven jet latitude as the latitude at which $\mathrm{U850_{max}}$ is measured. Prior to calculating these quantities, the mass streamfunction at 500 hPa and the zonal wind profile at 850 hPa are cubically interpolated at a resolution of 0.1° latitude. We choose the 850-hPa level to measure eddy-driven winds to avoid effects of topography on the surface winds, although we verified that the results of our analysis are nearly unchanged if surface winds are used.

d. Power spectrum of eddy momentum flux

The power spectra of eddy momentum flux at 250 hPa in the SH are calculated as a function of latitude and phase speed, using data from the preindustrial control integration of the GFDL-ESM2G model. First, the space–time cospectral power density is calculated at each latitude as in Hayashi (1971), using 120-day DJFM and JJAS time series tapered by a Hanning window. Following Randel and Held (1991), the wavenumber–frequency spectra are then transformed into wavenumber–phase speed space, and the contributions from all wavenumbers are added to obtain the power density as a function of phase speed at each latitude. The effect of interannual variations in $\mathrm{U850_{max}}$ on the spectral density of eddy momentum flux is estimated by regression analysis.

The same calculations are performed on 1948–2012 NCEP data, but to increase the number of samples used in the regression analysis, the seasons are further subdivided into 40-day time series (with three consecutive time series per season), yielding 192 samples. Because the lowest resolved phase speed depends on the length

TABLE 1. List of CMIP5 models used in our analyses. A cross × indicates that the data were available at the time of writing. Unless otherwise noted, the historical data cover the time period 1901–2005, and the RCP8.5 integrations span the period 2006–99.

	Model name	Model name expansion	Historical	RCP8.5
1	BCC-CSM1.1	Beijing Climate Center Climate System Model, version 1.1	×	×
2	CanCM4	Fourth generation Canadian Coupled Global Climate Model	1961–2005	
3	CanESM2	Second generation Canadian Earth System Model	×	×
4	CCSM4.0	Community Climate System Model, version 4.0	×	×
5	CNRM-CM5	Centre National de Recherches Météorologiques Coupled Global Climate Model, version 5	×	×
6	CSIRO Mk3.6.0	Commonwealth Scientific and Industrial Research Organisation Mark, version 3.6.0	×	×
7	FGOALS-g2	Flexible Global Ocean–Atmosphere–Land System Model, gridpoint, version 2	×	×
8	FGOALS-s2	Flexible Global Ocean–Atmosphere–Land System Model, second spectral version	×	×
9	GFDL CM3	Geophysical Fluid Dynamics Laboratory Climate Model, version 3	×	
10	GFDL-ESM2G	Geophysical Fluid Dynamics Laboratory Earth System Model with GOLD ocean component (2G)	×	
11	GFDL-ESM2M	Geophysical Fluid Dynamics Laboratory Earth System Model with MOM4 ocean component (2M)	×	×
12	GISS-E2-H	Goddard Institute for Space Studies Model E, coupled with HYCOM ocean model	×	
13	GISS-E2-R	Goddard Institute for Space Studies Model E, coupled with Russell ocean model	×	×
14	HadCM3	Hadley Centre Coupled Model, version 3	×	
15	HadGEM2-CC	Hadley Centre Global Environmental Model, version 2 (Carbon Cycle)	×	×
16	HadGEM2-ES	Hadley Centre Global Environmental Model, version 2 (Earth System)	×	×
17	INM-CM4	Institute of Numerical Mathematics Coupled Model, version 4	×	×
18	IPSL-CM5A-LR	L'Institut Pierre-Simon Laplace Coupled Model, version 5A (low resolution)	×	×
19	IPSL-CM5A-MR	L'Institut Pierre-Simon Laplace Coupled Model, version 5A (medium resolution)	×	
20	IPSL-CM5B-LR	L'Institut Pierre-Simon Laplace Coupled Model, version 5B (low resolution)	×	
21	MIROC-ESM	Model for Interdisciplinary Research on Climate, Earth System Model	×	×
22	MIROC-ESM-CHEM	Model for Interdisciplinary Research on Climate, Earth System Model, Chemistry Coupled	×	×
23	MIROC4h	Model for Interdisciplinary Research on Climate, version 4 (high-resolution)	1950–2005	
24	MIROC5	Model for Interdisciplinary Research on Climate, version 5	×	×
25	MPI-ESM-LR	Max Planck Institute Earth System Model (low resolution)	×	×
26	MPI-ESM-P	Max Planck Institute Earth System Model (paleo mode)	×	
27	MRI-CGCM3	Meteorological Research Institute Coupled Atmosphere–Ocean General Circulation Model, version 3	×	×
28	NorESM1-M	Norwegian Earth System Model, version 1 (medium resolution)	×	×
29	NorESM1-ME	Norwegian Earth System Model, version 1 (medium resolution, including interactive carbon cycle)	×	

of the time series, a wider range of phase speeds is unresolved as the time series are shortened. Nevertheless, we found this procedure to provide more reliable results in the regression analysis. Note that qualitatively similar results were obtained using 1979–2012 data only.

Because angular phase speed is conserved as a Rossby wave propagates meridionally, we represent the spectra as a function of $c_M = c/\cos\phi$ (angular phase speed c multiplied by Earth's radius $_a$), as in Chen and Held (2007).

3. Relationship between the eddy-driven jet and the Hadley cell extent

Using 18 historical integrations from the CMIP3 model archive and NCEP reanalysis data, Kang and Polvani (2011) demonstrated the existence of a strong correlation between the latitude of the eddy-driven jet and the extent of the HC in SH summer. In winter, however, the relationship was found to be much weaker and quite variable among models; the cause for the different behavior was unclear.

To review some of the main seasonal differences, we represent the mean zonal and meridional circulation in the SH in Figs. 1 and 2, calculated from the NCEP reanalysis. In summer (DJFM), the zonal wind field is dominated by an eddy-driven jet centered near 50°S, and the subtropical jet only appears as a "shoulder" in the upper-tropospheric zonal wind profile (Fig. 1). In winter (JJAS), however, the subtropical jet is reinforced by the strong advection of angular momentum by the mean meridional circulation, and its core is collocated with the edge of the HC. The seasonality of the subtropical jet is related to the strong seasonal cycle of the HC, which reaches its peak strength in winter when the ascending branch is in the Northern Hemisphere. In summer, the Hadley and Ferrel cells are of comparable strength, suggesting that the summer HC is largely driven by eddies. The relative importance of eddy fluxes and of the mean meridional

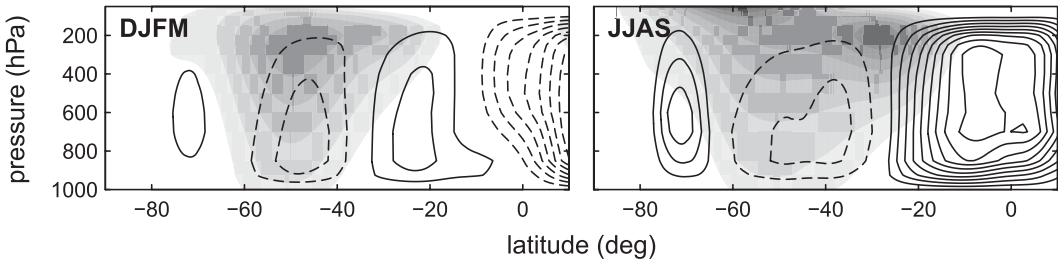


FIG. 1. Mean Southern Hemispheric zonal wind and mass streamfunction in the NCEP reanalysis (1948–2012). Shown are (left) DJFM and (right) JJAS. Zonal wind speeds are shaded in intervals of 5 m s^{-1} and wind speeds smaller than 5 m s^{-1} are not shaded, so that only westerly winds are represented. The contours denote the mass streamfunction, with clockwise (counterclockwise) circulation represented by dashed (solid) lines. The contour interval is 2×10^{10} kg s^{-1}, with the zero contour omitted.

circulation as a function of season has been studied by Schneider and Bordoni (2008), among others.

The 850-hPa zonal wind, which we use to determine the latitude and speed of the eddy-driven jet, is represented in Fig. 2 as a function of latitude and longitude. The eddy-driven jet is highly zonally symmetric in the Southern Hemisphere, particularly in DFJM; it features an annular structure with maximum wind speeds near 50°S in both seasons. The jet tends to be wider in JJAS, especially in the Pacific basin, where the westerly winds extend toward the subtropics.

In Fig. 3 we repeat the analysis carried out by Kang and Polvani (2011), but using the eddy-driven jet speed $U850_{max}$ instead of jet latitude. Both $U850_{max}$ and $\phi_{\Psi 500}$ were detrended by subtracting a least squares fit from the time series, and the mean was subtracted to obtain the anomalies $U850'_{max}$ and $\phi'_{\Psi 500}$. A significant positive correlation is found both in summer (multimodel mean: 0.65) and winter (0.52), with fairly similar values across models and in the reanalysis. (Note that $\phi_{\Psi 500}$ is defined in degrees south, so that a positive anomaly corresponds to an anomalously wide HC.) The correlations and slopes are summarized in Fig. 4. Contrary to what was observed with jet latitude, the correlations tend to be only slightly weaker in winter than in summer. However, the slopes are consistently smaller in winter, meaning that, for a given increase in $U850_{max}$, $\phi_{\Psi 500}$ increases much less in winter relative to summer. Note that the correlations and slopes were also calculated using 2006–2100 model output from RCP8.5 integrations, giving very similar results (not shown).

Our results have two main implications. First, the relationship between extratropical eddies and the extent of the HC does seem to be seasonally dependent, as implied by the different slopes in winter and summer. Second, the mere fact that the *speed* of the eddy-driven jet is correlated with the edge of the HC suggests that some property of the eddies may explain at least part of the interannual variations in HC width. We first explore the latter of these implications by investigating the

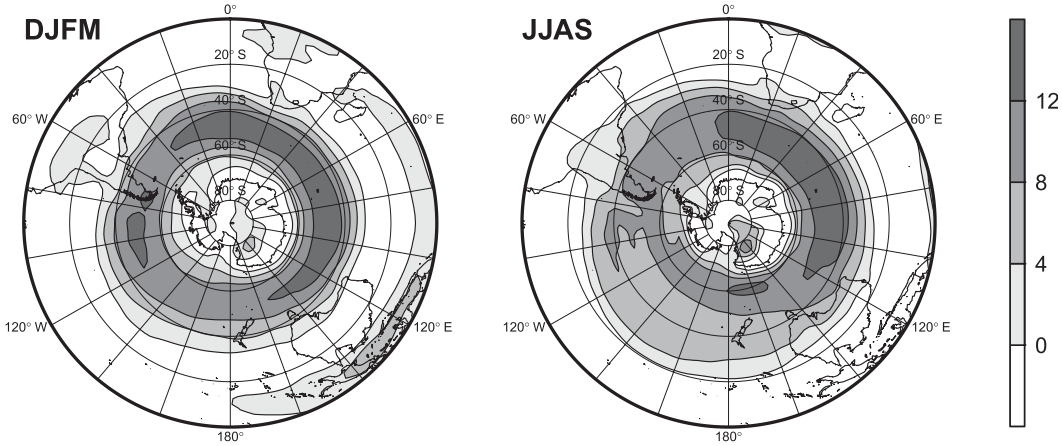


FIG. 2. Mean Southern Hemispheric zonal wind at 850 hPa in the NCEP reanalysis (1948–2012). Shown are (left) DJFM and (right) JJAS. Only westerly wind speeds are shaded in 4 m s^{-1} intervals.

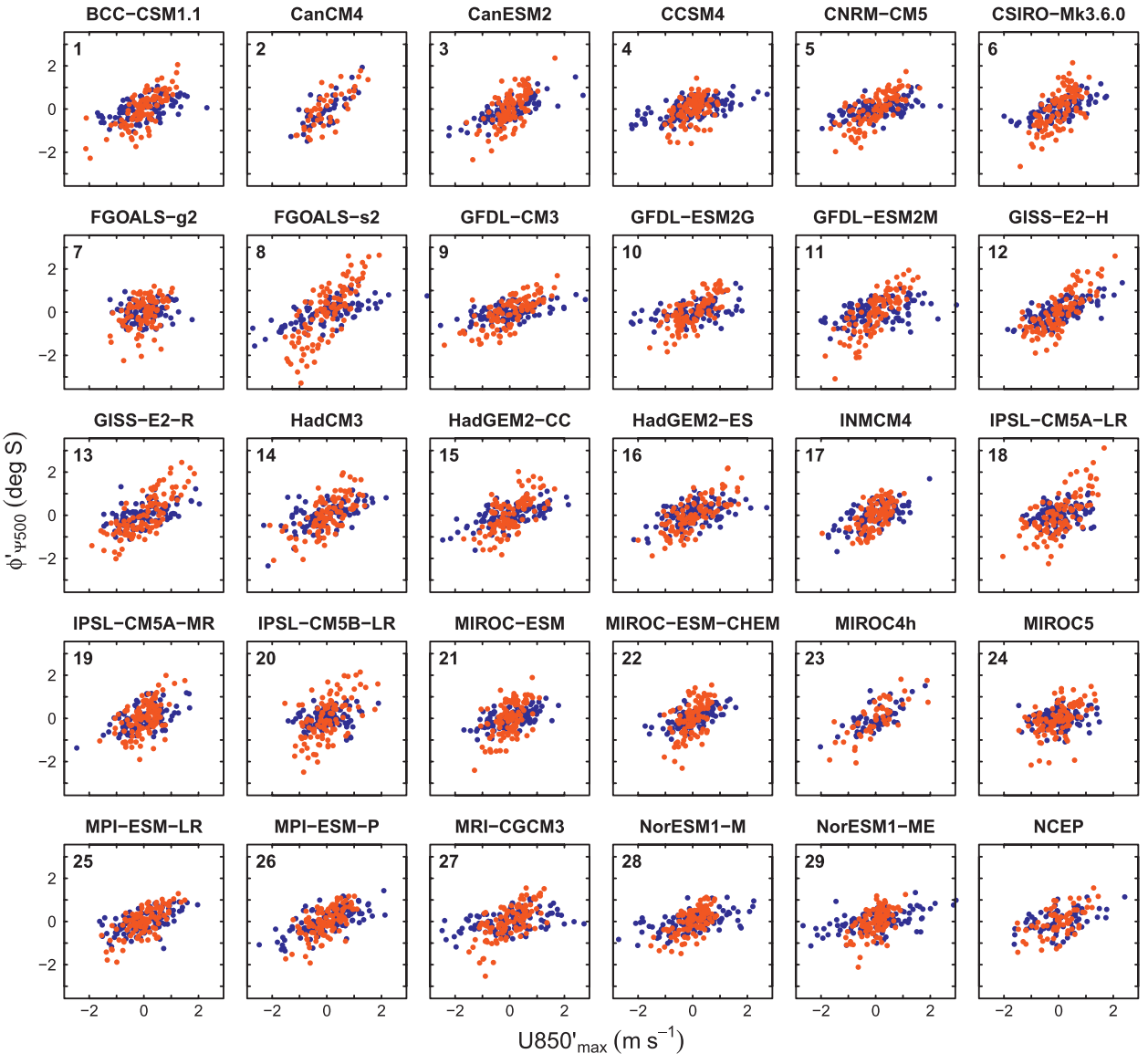


FIG. 3. Seasonal anomalies in eddy-driven jet speed $U850'_{max}$ and HC edge $\phi'_{\Psi 500}$ in the SH. Shown are historical integrations (June 1901 to March 2005) from the CMIP5 archive and the NCEP reanalysis (June 1948 to March 2012). Red is DJFM and blue is JJAS. The numbers refer to the models listed in Table 1.

relationship between the speed of the eddy-driven jet and the phase speed spectrum of eddies.

4. Effect of variations in eddy phase speeds

Midlatitude eddies can be described as Rossby waves that grow near the surface in regions of high baroclinicity and propagate both vertically and meridionally away from their source region (Edmon et al. 1980). In Mercator coordinates, the total wavenumber of a Rossby wave may be expressed as (Hoskins and Karoly 1981)

$$K^* = \left(\frac{\beta_M^*}{\overline{u}_M - c_M}\right)^{1/2},$$

where β_M^* is the meridional gradient of absolute vorticity on the sphere times the cosine of latitude, $\overline{u}_M = \overline{u}/\cos\phi$ is the Mercator mean zonal wind, and c_M is the phase speed of the wave. According to linear wave theory, such waves propagate toward higher values of K^* and experience a critical latitude where $\overline{u}_M = c_M$; there, K^* goes to infinity and wave breaking occurs. As shown by Randel and Held (1991), linear wave theory appears to provide a satisfactory explanation for the observed patterns of

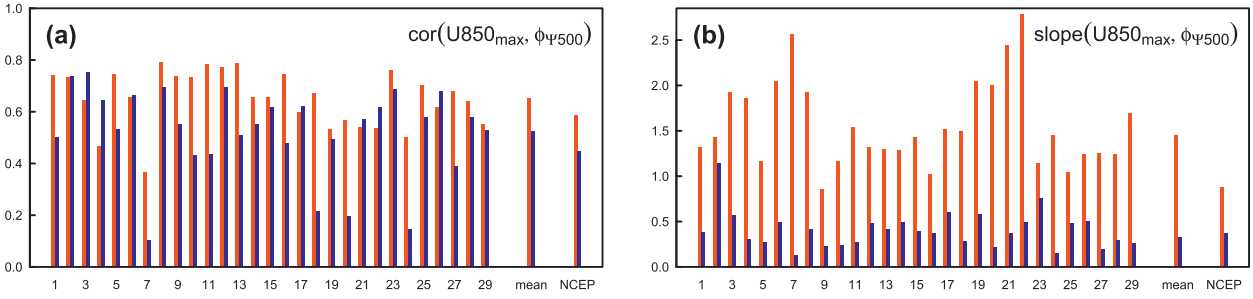


FIG. 4. (a) Correlation between $U850_{max}$ and $\phi_{\Psi 500}$. (b) Slope of the total least squares fit to the ($U850_{max}$, $\phi_{\Psi 500}$) points. The numbers refer to the models listed in Table 1, and "mean" denotes the multimodel ensemble mean. Red is DJFM and blue is JJAS.

eddy propagation, as the distribution of wave drag is observed to be roughly parallel to the $\overline{u}_M = c_M$ line. Because the westerly zonal flow generally decreases as a wave travels away from the midlatitude jet, the critical latitudes are expected to depend on the phase speeds of the waves. For a wave propagating equatorward, this implies that higher phase speeds correspond to critical latitudes farther poleward. In other words, faster waves tend to break sooner as they travel away from their source region in midlatitudes.

Chen and Held (2007) and Chen et al. (2008) proposed that this mechanism may be key in explaining both interannual variations and long-term trends in the latitude of the eddy-driven jet. Using latitude–phase speed spectra of eddy momentum flux, they showed how changes in eddy phase speeds coincide with shifts of the jet, both in the reanalysis and in GCM simulations. They suggested that this is because equatorward-propagating waves break sooner as their phase speeds increase. Since most waves propagate toward lower latitudes because of the sphericity of the Earth, a shift in critical latitudes on the equatorward flank of the jet induces a shift in eddy momentum fluxes, which in turn affects the location of the eddy-driven jet.

We now consider the effect of shifts in the critical latitudes on the extent of the HC. In the upper troposphere, the steady-state, zonally averaged meridional flow approximately obeys the large-scale balance:

$$(f + \overline{\zeta})\overline{v} \approx \mathrm{div}(\overline{u'v'}\cos\phi), \qquad (1)$$

where f represents the Coriolis parameter, ζ denotes the relative vorticity, ϕ is latitude, and $\mathrm{div}(u'v'\cos\phi)$ is the divergence of meridional eddy momentum flux. Primes indicate eddy terms while overbars correspond to temporal and zonal averages. The neglected terms are the vertical advection terms as well as friction (see, e.g., Vallis 2006, Eq. 11.4). From Eq. (1) it is clear that the edge of the HC, where $\overline{v} = 0$, must approximately coincide with the latitude where the divergence of eddy momentum flux is zero. Because the divergence of eddy momentum flux is induced by the breaking of Rossby waves, a meridional shift of the critical latitudes may also affect the extent of the HC by shifting the meridional pattern of eddy momentum fluxes.

It is worth emphasizing that although such a mechanism could explain interannual variations and trends in HC extent, it cannot predict the *mean* extent of HCs. A classical model for idealized HCs in nearly inviscid flow was proposed by Held and Hou (1980). In this model, eddies are nonexistent, the HC is driven by meridional differences in diabatic heating, and the meridional extent of the HC is set by the constraints of angular momentum and energy conservation. While it demonstrates that baroclinic instability and eddies are not required to explain the finite extent of the HC, the Held–Hou model fails at quantitatively describing the mean state and variability of real-world HCs, in which the flow does not conserve angular momentum (Schneider 2006; Frierson et al. 2007). In the real world, the flow in the upper branch of the HC would become baroclinically unstable before the HC terminates, according to the Held–Hou scaling, because of the high westerly wind speeds and meridional shears (Schneider 2006; Frierson et al. 2007), and thus, eddies are likely key in explaining the width of real-world HCs. In the following sections of this paper, we will further investigate the relationship between eddies and interannual variations in HC extent.

5. Eddy phase speeds and speed of the midlatitude jet

We first address the question of how the jet speed relates to the phase speed of eddies. Figure 5 shows the mean seasonal power spectra of eddy momentum flux at 250 hPa for the preindustrial control integration of the GFDL-ESM2G model. The response to a change in jet speed is calculated by regressing the power spectra onto $U850_{max}$. It can be seen that when the eddy-driven jet is stronger, there is an increased occurrence of waves at anomalously high phase speeds. (Note that, because

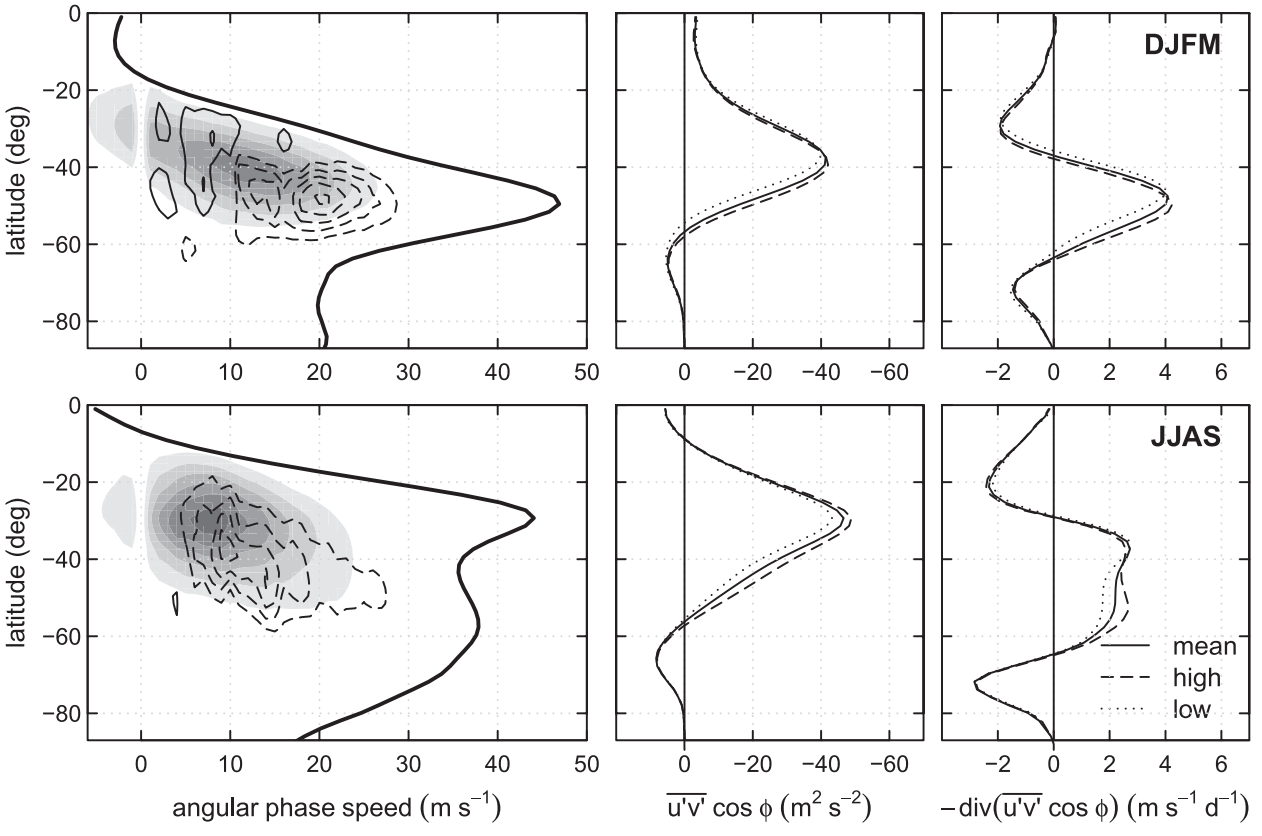


FIG. 5. (left) Power spectrum of eddy momentum flux at 250 hPa as a function of angular phase speed (multiplied by Earth's radius) and latitude in the preindustrial control integration of the GFDL-ESM2G model (500 years). Shading denotes mean values, while contours represent the regression coefficient of $U850_{max}$ onto the power spectrum. The shading interval is 0.2 m^2 s^{-2}, and values higher than -0.2 m^2 s^{-2} are not shaded. Low phase speeds that cannot be resolved are left unshaded. Positive contours are solid and negative contours are dashed, with a contour interval of 0.04; zero contours are omitted. The thick black line indicates the mean zonal wind at 250 hPa, divided by cosϕ for comparison. (middle) Eddy momentum flux at 250 hPa. Mean values are represented by a solid line, while dashed and dotted lines indicate composites over high and low values of $U850_{max}$, respectively (see text for details). (right) Mean and composited eddy momentum flux convergence at 250 hPa. Shown are (top) DJFM and (bottom) JJAS.

northward fluxes are defined as positive, the mean power is negative, so that negative anomalies imply an increase in poleward fluxes). The spectrum of eddy momentum flux is tilted toward higher latitudes as the phase speeds increase, following the profile of the mean zonal wind. Because of this tilt with latitude, an increased occurrence of faster waves goes along with an expansion of the power spectrum of eddy momentum flux toward higher latitudes.

We verified that the spectrum of phase speeds shifts toward higher values by calculating a power-weighted mean phase speed, averaged over all latitudes in the SH. We composited the power-weighted phase speed over seasons with high and low $U850_{max}$, defined as being at least one standard deviation away from the mean. The values are given in Table 2. In DJFM, the power-weighted phase speed increases by 1.8 m s^{-1}, from 10.6 to 12.4 m s^{-1}, while the increase is slightly more modest in JJAS. Note that in both seasons the change in power density is statistically significant at the 1% level in most of the contoured regions, based on the significance of the regression coefficient.

The results of the regression analysis indicate that as the eddy-driven jet strengthens, there is only a small decrease in power at lower phase speeds. This implies that a stronger jet coincides with an increased flux of momentum by the eddies from tropics to midlatitudes. To confirm this result, we consider the total eddy momentum flux $\overline{u'v'}\cos\phi$ and calculate composites over high and low values of $U850_{max}$, defined as above. The results, shown in the middle panels of Fig. 5, are consistent with our interpretation: when $U850_{max}$ is anomalously high, the total poleward eddy momentum fluxes increase, sustaining a stronger eddy-driven jet. Moreover, the increase occurs mainly near the peak and poleward thereof, while the fluxes in the tropics remain nearly unchanged. This induces a poleward shift of the peak of eddy momentum flux, mostly in DJFM. Through much of the subtropics

TABLE 2. Power-weighted eddy angular phase speeds (multiplied by Earth's radius) in the GFDL-ESM2G preindustrial control integration, composited over high and low values of $U850_{max}$ and the ENSO index (see text for details). All values are in meters per second.

		High	Low
$U850_{max}$	DJFM	12.4	10.6
	JJAS	11.3	10.3
ENSO index	DJFM	11.1	11.8
	JJAS	10.9	10.9

and midlatitudes, we found the total eddy momentum flux high and low composites to be significantly different from the mean at the 1% level by testing the difference between the groups at each latitude with the Wilcoxon rank-sum test (see, e.g., Hollander and Wolfe 1999).

It is also useful to consider the convergence of eddy momentum flux, which sustains the eddy-driven jet (Fig. 5, right). In DJFM, as $U850_{max}$ increases, the peak of convergence shifts poleward and the region of divergence expands, so that the transition from net divergence to convergence occurs at an anomalously high latitude. In JJAS, most of the change occurs between 40° and 60°S, where there is increased convergence when $U850_{max}$ is higher. In the high phase, the meridional distribution of eddy momentum flux convergence becomes bimodal, with the appearance of a peak near 50°S. This bimodality has been discussed in detail by Codron (2007) and arises mostly from the presence of a strong subtropical jet in the Pacific sector (see also Barnes and Hartmann 2011).

Now turning to the results from the NCEP reanalysis (Fig. 6), we note that the results are qualitatively similar, but the signal in the power spectrum is weaker. This is likely because the eddy phase speed spectra for individual seasons are noisy and the time series is relatively short. Nevertheless, the results are consistent with the interpretation provided above, and the composites of total eddy momentum flux and eddy momentum flux convergence (Fig. 6, middle and right) are very similar relative to the GCM results.

From this analysis we obtain a clear picture of the relationship between jet speeds and eddy phase speeds. On average, a stronger jet is sustained by increased poleward eddy momentum fluxes from the tropics; the increased flux is provided by the additional contribution of anomalously fast waves. As the flux increases, the peak of eddy momentum flux is displaced poleward, coincident with a poleward expansion of the region of divergence. The anomalous divergence is balanced by anomalous meridional winds, consistent with a wider HC.

As discussed in section 4, the latitude where $\mathrm{div}(\overline{u'v'}\cos\phi) = 0$ in the subtropics (corresponding to the peak of poleward eddy momentum flux) is expected to approximately coincide with the edge of the HC. To verify that this is the case, the two quantities are plotted against each other in Fig. 7. On interannual time scales, the variations are well correlated, particularly in DJFM, where the variability in HC extent is largest. The dots are also close to the one-to-one line. Thus, interannual variations in the meridional distribution of eddy momentum flux convergence and divergence agree well with the variability of the HC width.

6. Effect of ENSO

A well-known factor of interannual variability of the HC is ENSO. In the warm ENSO phase, both the HC and the eddy-driven jet tend to be shifted equatorward relative to their mean position, while the opposite happens during the cold ENSO phase (Seager et al. 2003; Chen and Held 2007; Lu et al. 2008). To first order and in the zonal mean, this variability is hemispherically symmetric. In this section, we briefly discuss how the ENSO-induced variability differs from that induced by variations in eddy phase speeds. A similar and more detailed discussion of these differences has been provided by Chen and Held (2007) and Lu et al. (2008).

We regress the power spectrum of eddy momentum flux at 250 hPa onto an ENSO index in the GFDL-ESM2G preindustrial control integration (Fig. 8). The values of the ENSO index are calculated as the anomalies in sea surface temperature averaged over a domain in the east equatorial Pacific (5°S–5°N, 120°–170°W), consistent with the definition of the Niño-3.4 index (Trenberth 1997). The response to changes in the ENSO index have a dipolar structure in DJFM, such that the warm ENSO phase corresponds to an equatorward shift of the spectrum and vice versa (recall that negative anomalies imply an increase in power). In JJAS, the response is mostly a decrease in power on the poleward side of the spectrum as the ENSO index increases. In both cases, no clear change appears in the distribution of eddy phase speeds in relation to ENSO, and changes in the power-weighted phase speeds are modest (Table 2). Rather, the meridional shift of the power spectrum likely results from changes in the mean zonal wind, as discussed by Chen et al. (2008) and Lu et al. (2008). During warm ENSO events, the tropics warm, sustaining stronger subtropical zonal winds by thermal wind balance. The increase in mean zonal wind induces changes in the index of refraction, so that the critical latitudes of extratropical waves are shifted equatorward. The reverse happens during cold ENSO events. This mechanism is consistent with the changes in the subtropical index of refraction observed by

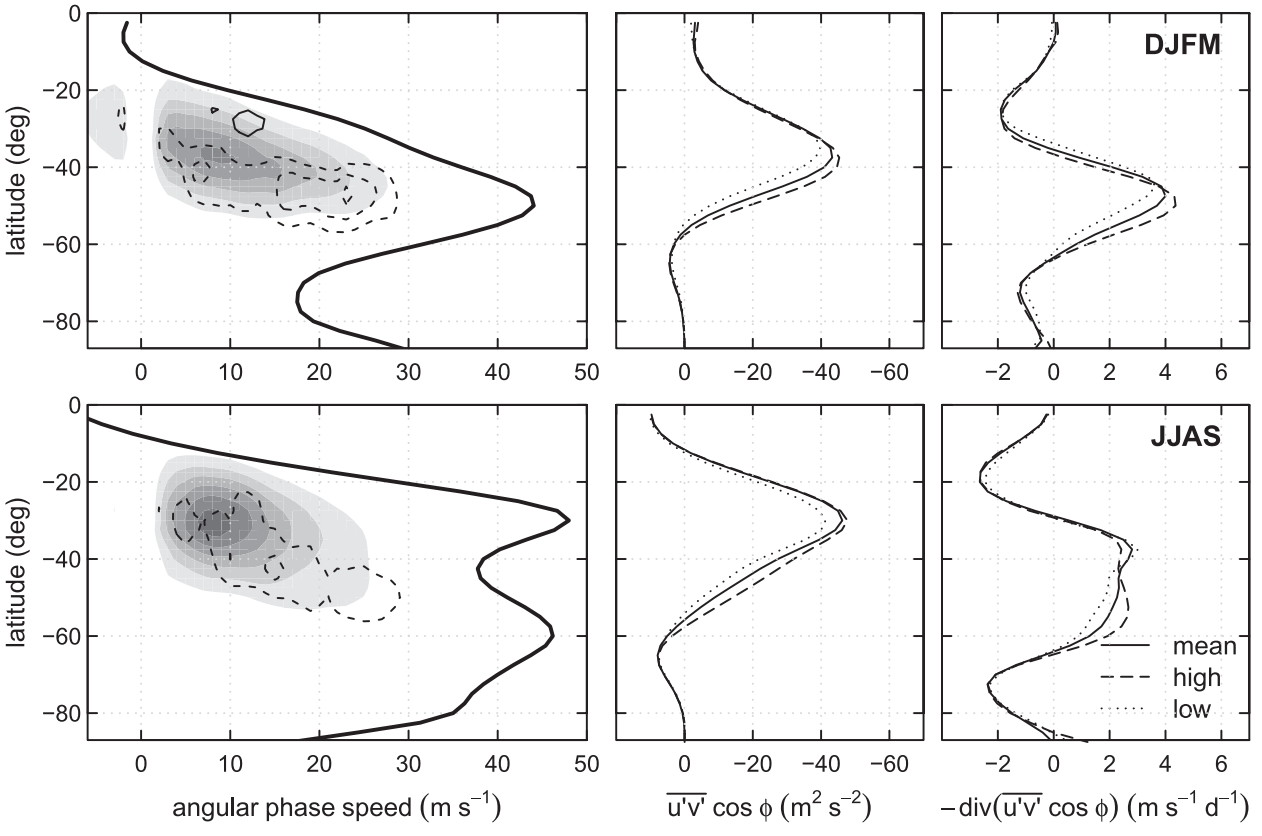


FIG. 6. As in Fig. 5, but for the NCEP reanalysis from June 1948 to March 2012 (64 years). The range of unresolved phase speeds is broader than in Fig. 5 because of the shorter data subsets used (40 vs 120 days; see section 2).

Seager et al. (2003). By the same arguments as before, the shift in the distribution of eddy momentum flux convergence and divergence induces a shift of the edge of the HC.

In summary, the ENSO-induced variability of the HC width is related to changes in mean zonal wind in the subtropics; this differs from the variability induced by changes in eddy phase speeds. However, both share the common feature of inducing shifts in the critical latitudes of extratropical waves. These two different types of variability are likely superimposed, but our results seem to indicate that on interannual time scales, the signal caused by the phase speed–induced variability dominates.

7. Variability of the Hadley cell width

We now turn to the first of the implications we deduced from our results in section 3, which is how the effect of eddies on the HC width depends on season. As could be determined from visual inspection of Figs. 3 and 7, the variability of the extent of the HC is much larger in DJFM than in JJAS. Moreover, in Fig. 4b, we observed that the HC width is less sensitive to changes in $U850_{max}$ in JJAS than in DJFM. In the following, we provide an interpretation in the context of linear wave theory.

Figure 9 (left) shows the mean zonal wind at 250 hPa from 50° to 10°S. Because of the strong seasonal cycle of the subtropical jet, the meridional gradient of the mean zonal wind maximizes in SH winter and reaches a minimum in the summer. As discussed in section 4, linear wave theory predicts that Rossby waves break where $\overline{u} = c$. This has an important implication: for a given change in c, and assuming the zonal wind remains constant, the latitudinal shift of the critical line will be inversely proportional to the meridional gradient of the upper-tropospheric zonal wind, $\partial/\partial y$(U250). In other words, when $\partial/\partial y$(U250) is large, as in JJAS, an increase in c only induces a slight shift of the critical line because $\overline{u}$ changes rapidly with latitude; the opposite is true if $\partial/\partial y$(U250) is small.

Assuming that $U850_{max}$ is correlated with the mean phase speed of the waves, this hypothesis provides an explanation for the observed seasonal variations in the slope of the ($U850_{max}$, $\phi_{\Psi 500}$) relationships (cf. Fig. 4).

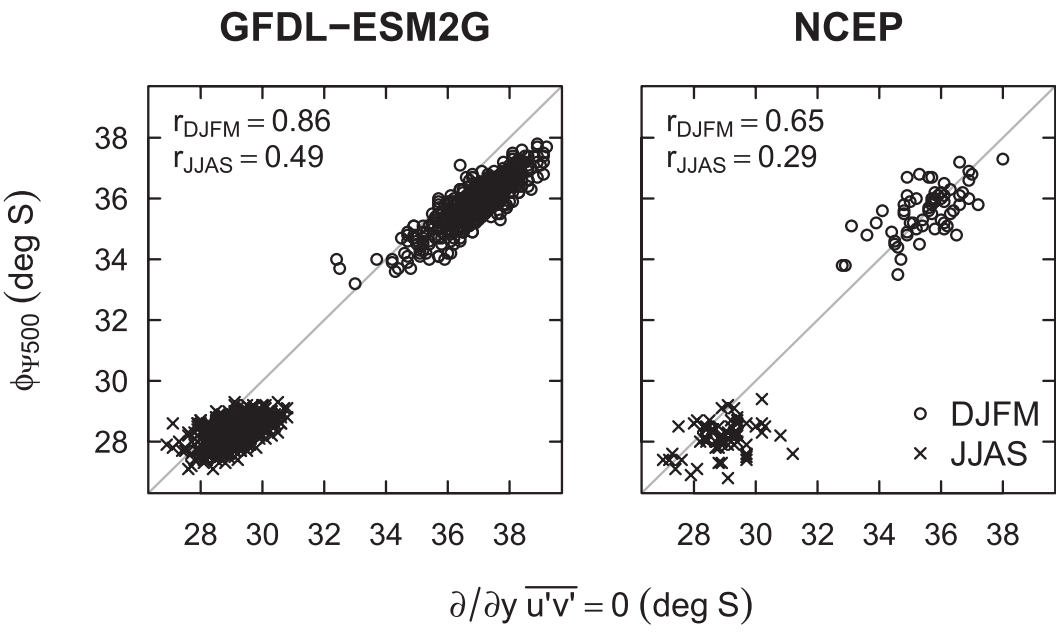


FIG. 7. Edge of the HC vs latitude where $\mathrm{div}(\overline{u'v'}\cos\phi) = 0$. Shown are (left) the preindustrial control integration of the GFDL-ESM2G model and (right) the NCEP reanalysis. Each point represents a season.

We further verify this by calculating the full seasonal cycle of the ($U850_{max}$, $\phi_{\Psi 500}$) slopes in the GFDL-ESM2G preindustrial control integration and comparing the slopes with the seasonal cycle of $\partial/\partial y$(U250). The slopes and meridional wind gradients were calculated for each month of the year. The meridional wind gradient is taken at the latitude of peak eddy momentum flux divergence (black curve in Fig. 9, left), assuming that most wave breaking occurs around that latitude (Barnes and Hartmann 2012). As shown in the right panel of Fig. 9, the slopes of ($U850_{max}$, $\phi_{\Psi 500}$) are approximately linearly related to $[\partial/\partial y(\mathrm{U250})]^{-1}$ over the course of the seasonal cycle, with a maximum in summer and a minimum in winter {note that we plot the inverse of the meridional zonal wind gradient $[\partial/\partial y(\mathrm{U250})]^{-1}$ so that both variables have the same units of degrees latitude over meters per second}.

Along with the latitude of peak divergence, we also represented the critical line in Fig. 9 for an eddy angular phase speed of 11 m s^{-1}, which is close to the mean power-weighted phase speed (see also Table 2). Although the seasonal cycles look very similar, the critical line is systematically several degrees equatorward of the line of peak divergence, particularly in JJAS where the meridional wind shear is strong. The fact that meridionally propagating waves generally do not reach their critical latitudes has been noted in previous studies (Feldstein and Held 1989; Randel and Held 1991), and this likely explains the discrepancy between the critical line and the line of peak divergence in our results.

The mechanism proposed here provides a simple explanation for the observed seasonal differences in interannual variability of the HC width. It also offers a possible interpretation of differences in long-term trends, which we shall discuss in section 9.

8. Eddy-driven jet latitude and speed

If the speed of the eddy-driven jet is indeed related to the mean eddy phase speeds of the eddies, then, following the Chen and Held (2007) hypothesis, it should correlate well with the latitude of the eddy-driven jet. The two quantities are plotted against each other in Fig. 10, again comparing the GFDL-ESM2G preindustrial control integration with the NCEP reanalysis. First, we note that the model and the reanalysis yield very similar results. The only exception is that the distribution is shifted toward higher wind speeds in the reanalysis, the cause for which is unclear. Now, considering seasonal differences, there is indeed a strong correlation between jet latitude and speed in DJFM, such that when the eddy-driven jet is stronger than average, it is also at an anomalously high latitude. In JJAS, however, the shape of the distribution is more complex. The jet latitude does tend to increase as its speed goes up, but for low jet speeds the jet has two preferred latitudes: one just poleward of the subtropical jet near 40°S and another in midlatitudes around 55°S. This is in agreement with the distribution of eddy momentum flux convergence, which tends to peak at these two latitudes (cf. right panels of

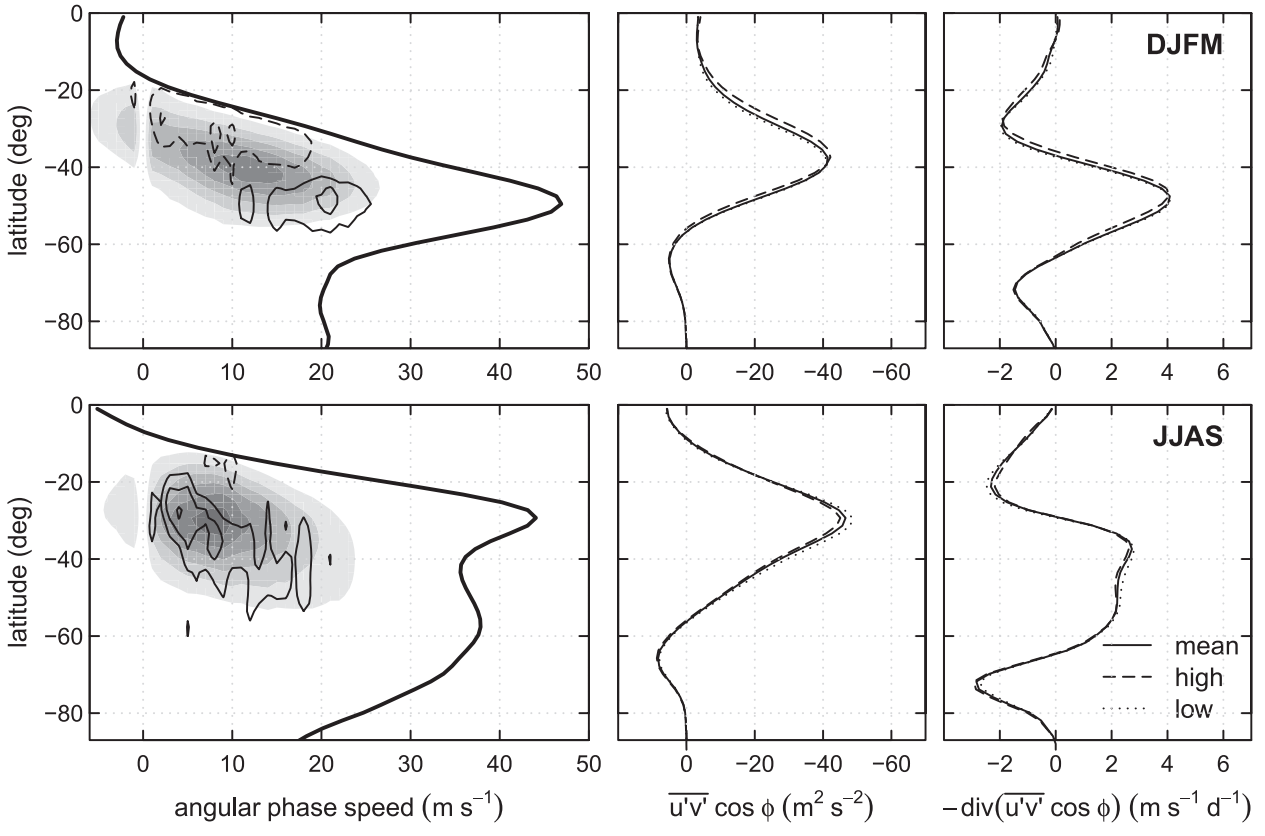


FIG. 8. As in Fig. 5, but regressing the phase speed spectrum onto the ENSO index for the GFDL-ESM2G preindustrial control integration.

Figs. 5, 6). The complex behavior of the jet in JJAS may explain the lack of correlation between jet latitude and HC width found by Kang and Polvani (2011). It is also interesting to note that, while the variability of the HC edge is larger in summer than in winter, the opposite is true of the jet latitude. Elucidating this contradiction is an interesting research question, but it goes beyond the scope of this paper.

It has been noted in several studies that the eddy-driven jet tends to strengthen as it shifts poleward (Chen

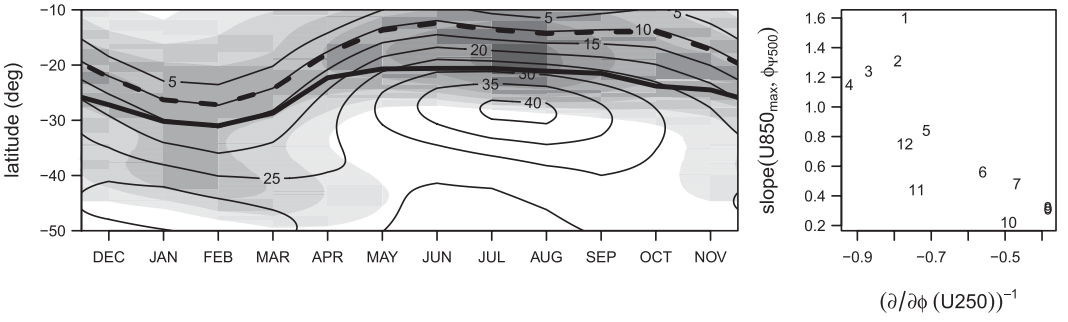


FIG. 9. (left) Mean zonal wind at 250 hPa U250 (contours) and meridional gradient of U250 (shading), plotted as a function of the month of the year for the preindustrial control integration of the GFDL-ESM2G model. The meridional gradient of U250 is shaded every 0.5 m s^{-1}°Lat^{-1}, and only values smaller that −0.5 m s^{-1}°Lat^{-1} are shaded. The thick solid line indicates the latitude of peak eddy momentum flux divergence, while the dashed line denotes the critical latitude for a wave with phase speed c_M = 11 m s^{-1} (see text). (right) Slope of the total least squares fit to (U850$_{max}$, $\phi_{\Psi 500}$) vs the inverse of the meridional gradient of U250 at the latitude of peak eddy momentum flux divergence. Both quantities are in degrees per meter per second. The plotted numbers refer to the respective month of the year.

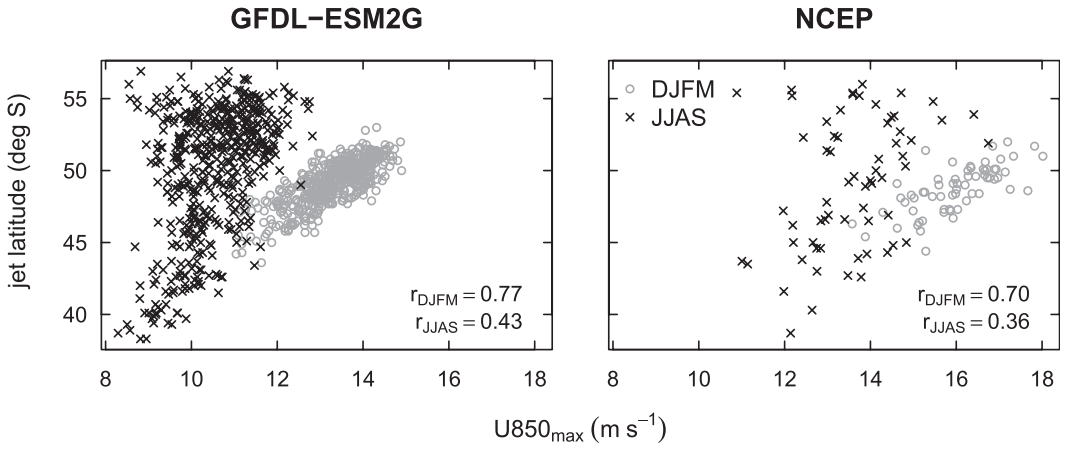


FIG. 10. Interannual variations in eddy-driven jet latitude vs speed in (left) the GFDL-ESM2G model and (right) the NCEP reanalysis.

and Held 2007; Lorenz and DeWeaver 2007). Using barotropic model experiments with varying drag, Kidston and Vallis (2012) also observed a relationship between jet latitude and speed and attributed it mainly to changes in wave propagation caused by a modified vorticity gradient on the jet flanks as the jet speed increases.

9. Trends

Given that interannual variations in eddy phase speeds appear to explain variations in HC extent, it is justified to ask whether long-term changes in phase speeds may explain the observed trends in HC width. Chen and Held (2007) demonstrated the existence of a positive trend in phase speeds in both the reanalysis and in twenty-first-century model simulations and linked those changes to a poleward shift of the eddy-driven jet. Assuming that trends in $U850_{max}$ reflect trends in the average phase speed of the eddies, we calculate trends in $U850_{max}$ and $\phi_{\Psi 500}$ by linear regression for each of the GCMs as well as for the ERA-Interim and NCEP reanalyses.

a. Hadley cell width

We first focus our attention on the trends in HC width only. In Fig. 11 (top), we show trends for 1979–2005 (26 years), which is the time period where the historical CMIP5 integrations and the reanalyses overlap; these trends are plotted in degrees latitude per decade. Trends in HC width are positive in most models in summer (DJFM), even though there is considerable spread among the models. Given the short time period over which the trends are calculated, much of the spread can likely be attributed to interannual variability. The two reanalysis datasets exhibit similar strong positive trends that are about 3 times larger than the multimodel mean. The positive trends in HC extent are consistent with findings from previous studies (see Seidel et al. 2008, and references therein). In winter (JJAS), most trends are not significant at the 5% level, and the mean trend is weakly positive. Here, the discrepancy between the reanalysis datasets is large. The stronger mean expansion in DJFM relative to JJAS is possibly caused by the effect of stratospheric ozone depletion, which has been shown to induce a poleward shift of the circulation (Polvani et al. 2011b; McLandress et al. 2011).

Projected trends for the twenty-first century (2000–99) are shown in Fig. 11 (bottom). These are based on the RCP8.5 emission scenario (Moss et al. 2010), with data for 2000–05 from the historical integrations. Nearly all models predict an expansion of the HCs in both winter and summer, and most trends are significant, particularly in winter. The spread in the rate of expansion is still considerable, especially in summer, but much smaller than for 1979–2005 (note the different scales between the top and bottom panels of Fig. 11).

b. Comparison with eddy-driven jet speeds

An interesting finding is that the trends in HC extent are roughly proportional to the trends in $U850_{max}$. For the historical period (Fig. 11, top), the distribution of points goes approximately through the origin, meaning that the trends tend to be directly proportional to one another. Also, the slopes are similar to those observed for interannual variations; again, for a given change in $U850_{max}$, the HC responds more strongly in summer than in winter. The same observations can be made for the twenty-first-century trends (Fig. 11, bottom). Thus far, the positive trend in mean eddy-driven jet speed has received surprisingly little attention in the literature.

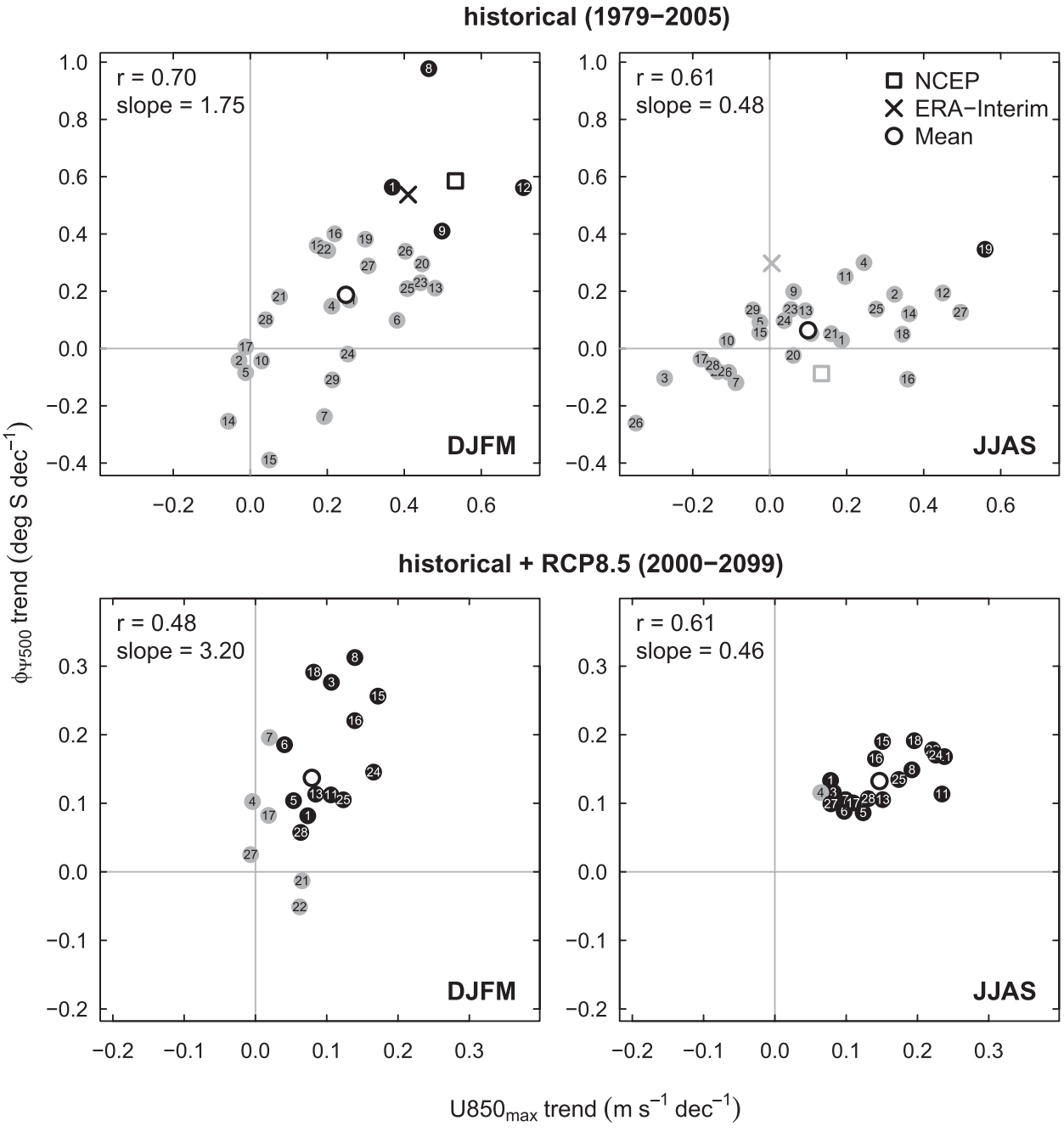


FIG. 11. The trend in $\phi_{\Psi 500}$ vs the trend in U850$_{max}$ for CMIP5 integrations as well as the NCEP and ERA-Interim reanalyses. Shown are (left) DJFM and (right) JJAS. (top) Historical CMIP5 integrations and reanalyses for 1979–2005. (bottom) Historical (2000–05) and RCP8.5 (2006–99) integrations for 2000–99. The RCP8.5 integrations start in December 2005 or January 2006, depending on the model. All trends are given in degrees latitude per decade. Models for which at least one of the trends is not significant at the 5% level are shown in gray. The numbers correspond to the models in Fig. 3; the open circle represents the multimodel ensemble mean, and the square and the cross denote the NCEP and ERA-Interim reanalyses, respectively. Note the different scales in the top and bottom panels.

Consistent results were obtained by Archer and Caldeira (2008), who found positive jet speed trends in the 40-yr ECMWF Re-Analysis (ERA-40) for December–February, and Kidston and Vallis (2012), who observed a correlation between trends in jet speed and latitude in CMIP3 integrations with increasing CO_2. However, both studies considered upper-tropospheric wind speeds. Further research is needed to understand the causes

behind the increase in mean jet speed and its relationship to eddy fluxes of momentum and heat.

It therefore appears that at least part of the differences in the rate of expansion of the HC among models can be related to differences in trends in $U850_{max}$. This result raises the question of whether a stronger HC expansion should be expected in summer, given the higher sensitivity to changes in eddy phase speeds. From Fig. 11, this does not appear to be the case for twenty-first-century projections, as the multimodel mean rates of HC expansion are of similar magnitude in winter and summer. An important factor that makes a comparison between the two seasons difficult is the expected recovery of the ozone hole. Greenhouse warming and ozone hole recovery have opposite effects on the width of the HC, and a number of recent studies have shown that their effects should nearly cancel each other out during much of the twenty-first century (Polvani et al. 2011a; McLandress et al. 2011). Since the effect of ozone depletion is strongest in DJFM, it is likely that the projected trends in that season are weaker than those that would be induced by global warming alone. Overall, we still find an expansion of the circulation in DJFM in spite of ozone recovery, but this result might be sensitive to the time period considered since the effects of ozone recovery and greenhouse gas increase may occur at different rates.

Furthermore, it is important to emphasize that even if changes in eddy phase speeds do induce trends in HC width, they are likely not the only cause. In particular, long-term changes in the temperature and zonal wind fields that affect the tropics preferentially may induce changes in HC width independently of changes in eddy phase speeds, as shown in section 6 for ENSO-related variability. Such changes may also be seasonally dependent.

10. Discussion and conclusions

Using both reanalysis data and CMIP5 model output, we show the existence of a significant relationship between the speed of the eddy-driven jet and the meridional extent of the Hadley circulation in the Southern Hemisphere. A detailed analysis of the latitude–phase speed spectrum of eddy momentum flux in the upper troposphere shows that the two variables are linked through changes in the phase speeds of eddies. A stronger eddy-driven jet coincides with an increased occurrence of anomalously fast eastward-propagating waves that tend to break at anomalously high latitudes. This induces a poleward expansion of the region of net eddy momentum flux divergence and a shift of the region of convergence toward higher latitudes. Because of the prevailing balance between eddy momentum flux divergence and the Coriolis effect of the mean meridional wind in the upper troposphere, the poleward expansion of the belt of eddy momentum flux divergence corresponds to a widening of the HCs. This mechanism is similar to that invoked by Chen et al. (2007), but we are considering the effect of changes in divergence on the width of the HCs.

Modulation of the HC width by eddy phase speed variations is also consistent with the observed seasonal differences in HC variability. In winter, the HC width is found to be less sensitive to changes in eddy-driven jet speeds, and the HC edge varies less on interannual time scales. Our results suggest that this is related to the stronger zonal wind gradient in the upper troposphere. For a given change in phase speeds, the critical latitudes shift less when the zonal wind gradient is stronger.

In addition, the relationship between eddy-driven jet speed and HC width observed on interannual time scales is found to hold for long-term trends as well. In general, models with a stronger increase in eddy-driven jet speed exhibit a stronger poleward shift of the HC edge. Also, the slope of the relationship between the trends is similar to that found for interannual variations. In twenty-first-century simulations based on the RCP8.5 emission scenario, nearly all models predict both a poleward shift of the HC and a strengthening of the eddy-driven jet.

Several mechanisms have been proposed in the literature to explain positive long-term trends in HC width in the context of climate change. In addition to the effect of eddy phase speeds discussed in this paper, some plausible candidates are stratospheric polar ozone depletion (McLandress et al. 2011; Polvani et al. 2011b) and static stability and tropopause height through their effect on subtropical baroclinicity (Frierson et al. 2007; Lu et al. 2007). It remains to be shown whether and how these mechanisms may be related to changes in eddy phase speeds. As proposed by Chen et al. (2008), temperature changes that induce an acceleration of the upper-tropospheric zonal winds in midlatitudes may be related to phase speed increases by increasing the vertical wind shear. This could be the case for stratospheric ozone depletion, which, by cooling the polar stratosphere, leads to stronger lower-stratospheric zonal winds by thermal wind balance. Increases in subtropical static stability, such as those predicted to occur because of the rising moisture content of a warming troposphere, seem less likely to be directly related to phase speed trends. Additional research is needed to improve our understanding of these different mechanisms and estimate their relative contributions as the climate changes.

Another important question is that of causality. Our results do not provide any direct evidence for the fact

that the HC width responds to changes in eddy phase speeds and not the other way around. However, the proposed mechanism seems plausible from a physical perspective, and it remains to be determined what could cause the observed increases in phase speeds if these were responding to a widening of the HC. In addition, the observed seasonal dependence, with its relation to the meridional gradient of the upper-tropospheric zonal wind, also seems to validate our hypothesis.

We carried out the same analysis for the Northern Hemisphere, but no clear relationships between the eddy-driven jet speed and the width of the HC were found. This is probably because of the existence of strong zonal asymmetries and the presence of monsoon circulations, which make the definition of the poleward edge of the HC difficult. The importance of stationary waves in the Northern Hemisphere may also complicate the relationship between transient eddies and the mean meridional circulation. A different approach may be needed to study the effect of eddies on the interannual variability and trends of the Northern Hemispheric HC.

Acknowledgments. The authors wish to thank Mike Wallace, Dargan Frierson, and Libby Barnes for many helpful discussions and for critical comments on an early version of this manuscript. We also thank Olivia Martius and one anonymous reviewer for valuable suggestions that helped improve this work. We acknowledge the World Climate Research Programme's Working Group on Coupled Modelling, which is responsible for CMIP, and we thank the climate modeling groups (listed in Table 1 of this paper) for producing and making available their model output. For CMIP, the U.S. Department of Energy's Program for Climate Model Diagnosis and Intercomparison provides coordinating support and led development of software infrastructure in partnership with the Global Organization for Earth System Science Portals. This work was supported by the National Science Foundation under Grant Atmospheric and Geospace Sciences (AGS) 0960497.

REFERENCES

Archer, C. L., and K. Caldeira, 2008: Historical trends in the jet streams. *Geophys. Res. Lett.,* **35,** L08803, doi:10.1029/2008GL033614.

Barnes, E. A., and D. L. Hartmann, 2011: Rossby wave scales, propagation, and the variability of eddy-driven jets. *J. Atmos. Sci.,* **68,** 2893–2908.

——, and ——, 2012: Detection of Rossby wave breaking and its response to shifts of the midlatitude jet with climate change. *J. Geophys. Res.,* **117,** D09117, doi:10.1029/2012JD017469.

Chen, G., and I. M. Held, 2007: Phase speed spectra and the recent poleward shift of Southern Hemisphere surface westerlies. *Geophys. Res. Lett.,* **34,** L21805, doi:10.1029/2007GL031200.

——, ——, and W. A. Robinson, 2007: Sensitivity of the latitude of the surface westerlies to surface friction. *J. Atmos. Sci.,* **64,** 2899–2915.

——, J. Lu, and D. M. W. Frierson, 2008: Phase speed spectra and the latitude of surface westerlies: Interannual variability and global warming trend. *J. Climate,* **21,** 5942–5959.

Codron, F., 2007: Relations between annular modes and the mean state: Southern Hemisphere winter. *J. Atmos. Sci.,* **64,** 3328–3339.

Dee, D. P., and Coauthors, 2011: The ERA-Interim reanalysis: Configuration and performance of the data assimilation system. *Quart. J. Roy. Meteor. Soc.,* **137,** 553–597, doi:10.1002/qj.828.

Edmon, H. J., B. J. Hoskins, and M. E. McIntyre, 1980: Eliassen-Palm cross sections for the troposphere. *J. Atmos. Sci.,* **37,** 2600–2616.

Feldstein, S. B., and I. M. Held, 1989: Barotropic decay of baroclinic waves in a two-layer beta-plane model. *J. Atmos. Sci.,* **46,** 3416–3430.

Frierson, D. M. W., J. Lu, and G. Chen, 2007: Width of the Hadley cell in simple and comprehensive general circulation models. *Geophys. Res. Lett.,* **34,** L18804, doi:10.1029/2007GL031115.

Hartmann, D. L., 1994: *Global Physical Climatology.* Academic Press, 411 pp.

Hayashi, Y., 1971: A generalized method of resolving disturbances into progressive and retrogressive waves by space fourier and time cross-spectral analyses. *J. Meteor. Soc. Japan,* **49,** 125–128.

Held, I. M., and A. Y. Hou, 1980: Nonlinear axially symmetric circulations in a nearly inviscid atmosphere. *J. Atmos. Sci.,* **37,** 515–533.

Hollander, M., and D. A. Wolfe, 1999: *Nonparametric Statistical Methods.* John Wiley, 787 pp.

Hoskins, B. J., and D. J. Karoly, 1981: The steady linear response of a spherical atmosphere to thermal and orographic forcing. *J. Atmos. Sci.,* **38,** 1179–1196.

Hu, Y., and Q. Fu, 2007: Observed poleward expansion of the Hadley circulation since 1979. *Atmos. Chem. Phys.,* **7,** 5229–5236, doi:10.5194/acp-7-5229-2007.

Johanson, C. M., and Q. Fu, 2009: Hadley cell widening: Model simulations versus observations. *J. Climate,* **22,** 2713–2725.

Kalnay, E., and Coauthors, 1996: The NCEP/NCAR 40-Year Reanalysis Project. *Bull. Amer. Meteor. Soc.,* **77,** 437–471.

Kang, S. M., and L. M. Polvani, 2011: The interannual relationship between the latitude of the eddy-driven jet and the edge of the Hadley cell. *J. Climate,* **24,** 563–568.

Kidston, J., and G. K. Vallis, 2012: The relationship between the speed and the latitude of an eddy-driven jet in a stirred barotropic model. *J. Atmos. Sci.,* **69,** 3251–3263.

Lorenz, D. J., and E. T. DeWeaver, 2007: Tropopause height and zonal wind response to global warming in the IPCC scenario integrations. *J. Geophys. Res.,* **112,** D10119, doi:10.1029/2006JD008087.

Lu, J., G. A. Vecchi, and T. Reichler, 2007: Expansion of the Hadley cell under global warming. *Geophys. Res. Lett.,* **34,** L06805, doi:10.1029/2006GL028443.

——, G. Chen, and D. M. W. Frierson, 2008: Response of the zonal mean atmospheric circulation to El Niño versus global warming. *J. Climate,* **21,** 5835–5851.

——, C. Deser, and T. Reichler, 2009: Cause of the widening of the tropical belt since 1958. *Geophys. Res. Lett.,* **36,** L03803, doi:10.1029/2008GL036076.

McLandress, C., T. G. Shepherd, J. F. Scinocca, D. A. Plummer, M. Sigmond, A. I. Jonsson, and M. C. Reader, 2011: Separating the dynamical effects of climate change and ozone depletion. Part II: Southern Hemisphere troposphere. *J. Climate,* **24,** 1850–1868.

Moss, R. H., and Coauthors, 2010: The next generation of scenarios for climate change research and assessment. *Nature,* **463,** 747–756, doi:10.1038/nature08823.

Polvani, L. M., M. Previdi, and C. Deser, 2011a: Large cancellation, due to ozone recovery, of future Southern Hemisphere atmospheric circulation trends. *Geophys. Res. Lett.,* **38,** L04707, doi:10.1029/2011GL046712.

——, D. W. Waugh, G. J. P. Correa, and S.-W. Son, 2011b: Stratospheric ozone depletion: The main driver of twentieth-century atmospheric circulation changes in the Southern Hemisphere. *J. Climate,* **24,** 795–812.

Randel, W. J., and I. M. Held, 1991: Phase speed spectra of transient eddy fluxes and critical layer absorption. *J. Atmos. Sci.,* **48,** 688–697.

Schneider, T., 2006: The general circulation of the atmosphere. *Annu. Rev. Earth Planet. Sci.,* **34,** 655–688, doi:10.1146/annurev.earth.34.031405.125144.

——, and S. Bordoni, 2008: Eddy-mediated regime transitions in the seasonal cycle of a Hadley circulation and implications for monsoon dynamics. *J. Atmos. Sci.,* **65,** 915–934.

Seager, R., N. Harnik, Y. Kushnir, W. Robinson, and J. Miller, 2003: Mechanisms of hemispherically symmetric climate variability. *J. Climate,* **16,** 2960–2978.

Seidel, D. J., Q. Fu, W. J. Randel, and T. J. Reichler, 2008: Widening of the tropical belt in a changing climate. *Nat. Geosci.,* **1,** 21–24, doi:10.1038/ngeo.2007.38.

Taylor, K. E., R. J. Stouffer, and G. A. Meehl, 2012: An overview of CMIP5 and the experiment design. *Bull. Amer. Meteor. Soc.,* **93,** 485–498.

Trenberth, K. E., 1997: The definition of El Niño. *Bull. Amer. Meteor. Soc.,* **78,** 2771–2777.

Vallis, G. K., 2006: *Atmospheric and Oceanic Fluid Dynamics.* Cambridge University Press, 745 pp.

Walker, C. C., and T. Schneider, 2006: Eddy influences on Hadley circulations: Simulations with an idealized GCM. *J. Atmos. Sci.,* **63,** 3333–3350.